Morphology, Deformation Behavior and Thermomechanical Properties of Polypropylene/Maleic Anhydride grafted Polypropylene/Layered Silicate Nanocomposites

I. L. Dubnikova,[1] S. M. Berezina,[1] Yu. M. Korolev,[2] G.-M. Kim,[3] S. M. Lomakin[4]

[1]*Semenov Institute of Chemical Physics, Russian Academy of Sciences, Moscow, 119991 Russia*
[2]*Topchiev Institute of Petrochemical Synthesis, Russian Academy of Sciences, Moscow, 119991 Russia*
[3]*Martin-Luther-University Halle-Wittenberg, Geusaer Straße, D-06217 Merseburg, Germany*
[4]*Emanuel Institute of Biochemical Physics, Russian Academy of Sciences, Moscow, 119991 Russia*

Received 24 May 2006; accepted 1 May 2007
DOI 10.1002/app.26665
Published online 11 June 2007 in Wiley InterScience (www.interscience.wiley.com).

ABSTRACT: Nanocomposites polypropylene (PP) with 3 and 7 wt % of clay were prepared by melt mixing. Four types of maleic anhydride grafted PP (MAPP) in broad range of MA groups content (0.3–4 wt %) and molecular weights (MW) were used as polar compatibilizers. The effect of the MAPP kind on both the clay dispersion and miscibility with PP was studied. The mixed intercalated/exfoliated morphologies of nanocomposites in the presence of all studied compatibilizers were revealed by XRD and TEM. The oligomer compatibilizer with 4 wt % of MA groups increases the intercalation ability of polymer into clay galleries but this one has limited miscibility with PP and worsens crystalline structure of polymer matrix. The MAPPs with 0.3–1.3% of MA are characterized by the lower intercalation ability but well cocrystallize with PP. Maximum reinforcing effect is attained using high MW MAPP with 0.6% MA and for nanocomposite with 7 wt % (3.8 vol %) of clay it averages almost 1.7 times relative to neat PP and 1.3 times relative to noncompatibilized composite. Dynamic storage moduli of nanocomposites compatibilized by MAPPs with 0.3–1.3% of MA containing 7 wt % of clay increase up to 1.4–1.5 around 30–75°C and over the whole temperature range remain higher compared with both neat PP and uncompatibilized composite. On the contrary, the oligomer MAPP with 4 wt % of MA groups decreases the thermal–mechanical stability of nanocomposite at high temperature compared with both PP and uncompatibilized composites. The study of nanocomposites flammability showed that creating complex composites containing both layered silicate and relatively small amount of magnesium hydroxide can be a successful approach to reduce the combustibility of PP-based nanocomposites. J Appl Polym Sci 105: 3834–3850, 2007

Key words: poly(propylene); composites; nanolayers; morphology; mechanical properties

INTRODUCTION

Nanocomposites based on polymers and layered silicates have attracted much interest in the last decade.[1–3] The interest in layered silicates as candidates for filler for the polymers is caused by their potential to exfoliate in the polymer matrix on single nanometric platelets (with aspect ratio from 50 to 150) as result of a penetration of macromolecules between the adjacent clay sheets.[4,5] To render hydrophilic silicates more compatible with polymers during melt blending, long-chain quaternary alkilammonium ions are used as organic modifiers for the clay.[6–8] The interlayer spacing d_{001} for pristine montmorillononite (MMT) particles is about 1 nm. The incorporation of organic cation between the adjacent clay platelets promotes an expansion of the interlayer distance up to 2.5–3 nm.[1] The polymer intercalation into the expanded interlayer galleries with the following clay exfoliation and homogeneous dispersion of the single-layered silicate platelets in the polymer matrix affords a basis for the production of polymer/layered silicate nanocomposites (PLSN) with markedly superior mechanical properties, barrier properties, improved heat distortion temperature (HDT), and fire resistance when compared with neat polymer.[9–12] It is important that such effects are achieved at low nanoscopic filler loading compared with conventional reinforcements; therefore, PLSNs combine low density and processability too. Generally, these effects were found for the polar polymers, compatible with hydroxyl groups of the silicate surface, e.g., nylon 6.[9–16] On the other hand, PLSNs based on the polyolefin polymers [polypropylene (PP), high density polyethylene (HDPE)] demonstrate lower improvement of

Correspondence to: I. L. Dubnikova (ild@chph.ras.ru).
Contract grant sponsor: Russian Foundation of Fundamental Research; contract grant number: 04-03-32052 and 06-03-08047.

Journal of Applied Polymer Science, Vol. 105, 3834–3850 (2007)

properties. Such nonpolar polymers poorly compatible with the mineral filler, and their intercalation into silicate galleries is difficult.[17–19] An approach had been suggested to improve the mixing of clay in PP using functional oligomer as compatibilizer, like maleic anhydride grafted PP (MAPP).[20,21]

Although many studies concerning the effect of the conditions of the preparation of polyolefin-based PLSN and the type of polar compatibilizer on the clay dispersion via the melt process have been reported, nevertheless, the compatibilizer optimal characteristics, such as grafting content and molecular weight, for the achievement of the exfoliated nanostructure and maximum improving properties of polyolefin/clay nanocomposites have not been clarified at present.[22–32] The purpose of this study was to better understand the influence of MAPP type on the polymer intercalation capability into the clay layers, miscibility with the bulk polymer matrix, and the properties of PLSNs. Four types of MAPP with broad range of MA contents and molecular weights (MWs) were used as polar compatibilizers during the preparation of nanocomposites by melt blending.

EXPERIMENTAL

Materials

Isotactic PP (Moscow Naphta Processing Plant, Russia) with a melt flow rate (MFI) = 0.6 g/10 min (2.16 kg, 230°C) was used as a matrix polymer ($M_w = 6.3 \times 10^5$ g/mol, $M_w/M_n = 3.5$). Organomodified montmorillonite Cloisite 20A (C20A) (Southern Clay Products), a power with a mean particle size of ~ 6 μm, was used as clay reinforcement (intercalant: dimethyl dihydrogenatedtallow ammonium chloride; intercalant content: 95 mEq/100 g clay; interlayer spacing: $d_{001} = 2.42$ nm). The four types of maleic anhydride-*graft*-PP with grafting contents of 0.3 (Exxelor PO2011), 0.6 (Polybond 3002), 1.3 (Polybond 3150), and 4 wt % (oligomer Licomont AR 504 with highest grafting content, $M_w = 2000$ g/mol) were used as compatibilizers. The compatibilizer codes, characteristics, and sources are listed in Table I. Both the MAPP**0.3** and MAPP**4** have lowest MWs.

Preparation of the nanocomposites by melt mixing

Composites were prepared by melt blending components in a two-roller mixing chamber (Brabender mixer) at a temperature of 190°C and a rotor rotation speed of 60 rpm. First, mixture of PP and MAPP was melt blended for 3 min. The clay was then added slowly for 3 min, and the mixture was compounded for 10 min. Thermal stabilizers topanol (0.3 wt %) and dilauriltiodipropionate (0.5 wt %) were used. The composites of three kinds were prepared based on neat PP without compatibilizer (PP/C20A), maleated PPs (MAPP/C20A), and PP with compatibilizer (PP/MAPP/C20A). The polymer blends of PP with polar MAPP (without clay) were prepared under similar conditions. For comparison, the unmodified PP was also processed in the mixer. The filler loadings in the composites were 3 and 7 wt % (1.6 and 3.8 vol %). The weight ratio of MAPP to C20A was equal to three.

Specimen preparation

The specimens for morphological and mechanical testing as 0.5-mm-thick plates were compression molded. The molding procedure involves heating at 190°C for 5 min without applied pressure and then for 5 min under pressure (10 MPa). The mold was cooled to 90°C by water at a rate of 16°C/min under pressure whereupon the sample was removed from the press.

Structural characterization

X-ray diffraction

The intercalation capability of the polymers into the C20A galleries was evaluated by monitoring the clay interlayer spacing by using X-ray diffractometer as follows. X-ray diffraction (XRD) analysis of the specimens was carried out using a DRON-2 computer-aided diffractometer (Cu Kα radiation, modified collimation) in the reflection mode using film samples. Measurements were performed at room temperature in the angular range $2\theta = 0.5°$–$40°$. Interlayer spacings in C20A were calculated from angular positions of basal reflections (00*l*) of C20A on the composite dif-

TABLE I
The Characteristics of Used Maleic Anhydride Grafted Polypropylenes

Compatibilizer, trade name	MA content (wt %)	Code	MFI, [a] g/10 min	T_m (°C)	Source
Exxelor PO2011	0.3	MAPP0.3	162	161	Exxon Chemical Co.
Polybond 3002	0.6	MAPP0.6	12	162	Uniroyal Chemical Co. Inc, Crompton Co.
Polybond 3150	1.3	MAPP1.3	43	159	Uniroyal Chemical Co. Inc, Crompton Co
Licomont AR 504	4	MAPP4	Wax	138; 150	Clariant GmbH Co.

[a] $H = 2.16$ kg; $T = 230$°C.

fractograms using the Bragg's relation: $\lambda = 2d \sin \theta$, where λ corresponds to the wave length of the X-ray radiation used in the diffraction experiment, d is the spacing between diffractional lattice planes, and θ is the measured diffraction angle.

Transmission electron microscopy

Ultrathin sections of the nanocomposites with a thickness of about 50 nm were microtomed at -80°C, using a Reichert-Jung Ultracut with diamond knife, and then investigated by a transmission electron microscope (TEM, JEOL 200CX), using an acceleration voltage of 200 kV without any chemical staining.

Atomic force microscopy

Atomic force microscopy (AFM) studies were performed with commercial scanning probe microscope Nanoscope IIIA and IV MultiMode (Digital Instruments/Veeco Metrology Group, USA) in tapping mode, at ambient conditions. Conventional etched Si probes (stiffness $\sim$ 40 N/m, resonant frequency 160–170 kHz) were used. The amplitude of the free-oscillating probe, A_0, varied in the 10–20 nm range while the set-point amplitude, A_{sp}, ranged from 0.5 to 0.8 A_0. Imaging was conducted on the flat sample surfaces being prepared at -80°C with an ultramicrotome MS-01 (MicroStar, USA) equipped with a diamond knife. Height and phase images were simultaneously recorded on polymer surfaces. Phase images provide a sharp contrast of fine structural features and emphasize differences in mechanical properties of different sample components.

Differential scanning calorimetry

The thermal characteristics of the neat PP and the PP matrix in composites were analyzed by differential scanning calorimetry (DSC), using PerkinElmer DSC-7 calorimeter. Measurements were made in the 25–180°C range at a heating rate of 10°C/min. The nonisothermal crystallization behavior of PP, MAPPs, polymer blends, and nanocomposites was studied at a constant cooling rate of 10°C/min.

Tensile test

Dumbbell specimens for mechanical testing were cut from 0.5-mm-thick molded sheets. The specimen dimensions were $0.5 \times 5 \times 30$ mm^3. Tensile modulus, yield stress and strain, stress and elongation at break were measured at ambient temperature, using a tensile testing machine (Instron-1122) with a crosshead speed of 20 mm/min (0.67 min^{-1}). The average values were calculated from eight runs for each specimen.

Dynamic mechanical analysis

Dynamic mechanical characteristics of samples in the form of 300-μm-thick films were obtained using a DMA Q800 (''Intertech Corporation'' TA Instruments) by sinusoidally vibrating the sample in the tensile mode at the frequency $f = 10$ Hz and a heating rate of 2°C/min. The temperature range was between -40 and 160°C.

Impact tests

The impact strength of notched specimens was measured at ambient temperature by Izod. Impact tests were carried out at 2.9 m/s on rectangular bars 80 mm $\times$ 10 mm $\times$ 4 mm with a single-edge 45° V-shaped notch (tip radius 0.25 mm, depth 1.5 mm). The average values were calculated from eight runs for each specimen.

Scanning electron microscopy

The microdeformation processes in nanocomposites were studied by scanning electron microscopy of the tensile deformed film surfaces, using EMPA ''Camebax'' MBX-1 (Cameca). All specimens were gold-sputtered before SEM analysis.

Cone calorimeter testing

The combustibility of PP nanocomposites was evaluated on a Dark Star Research Cone Calorimeter at 35 kW/m^2 heat flux and exhaust flow of 24 L/s, using the standardized cone calorimeter procedure (ASTM E-1354-92). Sample area was 7×7 cm^2, and sample mass was 13.5 ± 0.5 g. Data collected are the average of two samples, with an error of 10%.

RESULTS AND DISCUSSION

Evaluation of the intercalation capability of the MAPPs in MAPP/C20A composites

First of all, we studied the intercalation capability of the maleic anhydride functionalized PPs in the MAPP/C20A composites (where MAPP is the polymer matrix) depending on the grafting content and MW of the MAPP. The level of the polymer intercalation in a clay powder was evaluated on the basis of the change of the clay interlayer spacing from the 2θ position of the (001) diffraction peak. X-ray diffractograms of the C20A and composites with 3 wt % organoclay are presented in Figure 1(a). XRD analysis indicates the formation of intercalated nanocompo-

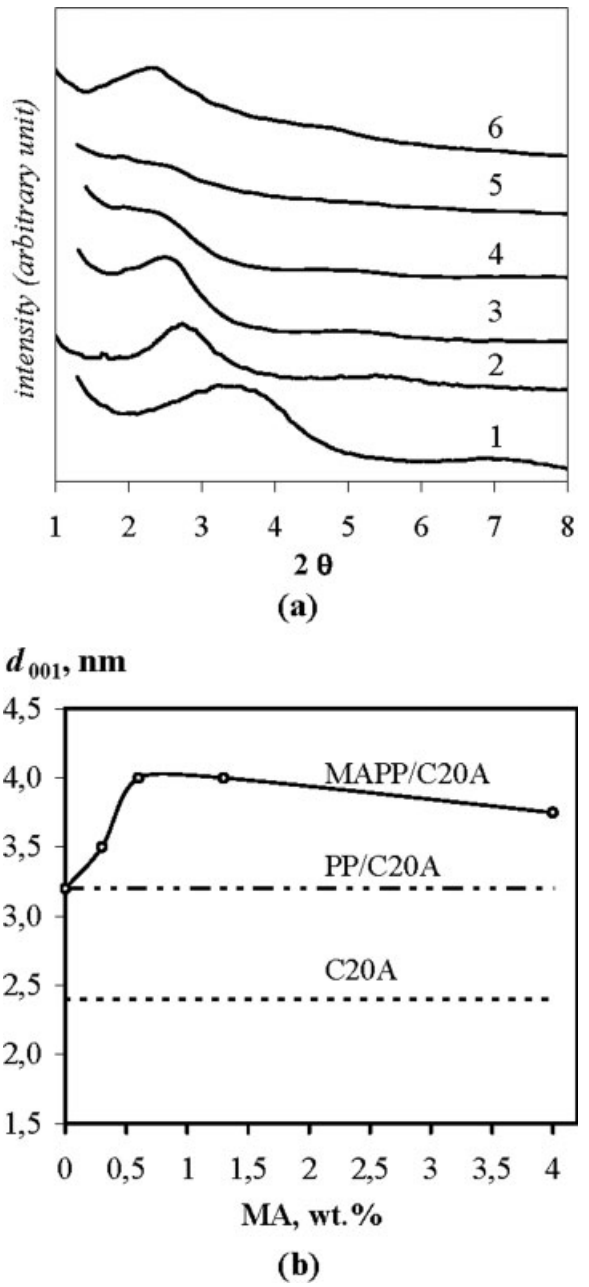

Figure 1 (a) WAXD patterns of organo clay C20A (1), composite PP/C20A (2) and nanocomposites MAPP0.3/C20A (3), MAPP0.6/C20A (4), MAPP1.3/C20A (5), and MAPP4/C20A (6). C20A content is 3 wt %. (b) The dependence of basal spacing d_{001} upon the MA content for MAPP/C20A nanocomposites as compared with that of as-received organo clay C20A and the PP/C20A.

sites. The dependence of the clay interlayer spacing d_{001} upon MA content for the MAPP/C20A composites is shown in Figure 1(b) when compared with the d_{001} in pristine organoclay and the PP/C20A composite based on neat nonpolar PP. The interlayer spacing of the C20A averages $d_{001} = 2.4$ nm. In the PP/C20A composite, the (001) peak is shifted to a lower angle and the interlayer distance increases accordingly to 3.2 nm. A distinct shift of the clay basal peak to a still lower angle is observed for the nanocomposites with the MAPP matrices as the grafting content increases; in other words, the intercalation capability of polymers increases with increasing their polarity. The interlayer spacing expands at most up to 4 nm with the increase of the MA content to 1.3 wt % [Fig. 1(b)]; at the same time, the increase in d_{001} value is accompanied by a significant decrease in the intensity of the basal peak. Hence, we can conclude that disorder or exfoliated regions form in the MAPP1.3/C20A nanocomposite. The presence of the single-layered silicate platelets in this nanocomposite was confirmed by TEM analysis (Fig. 2). An appreciable increase in the grafting content to 4 wt % leads to the minor decrease in the d_{001} value that can be related with a difficulty of the polymer chains diffusion into the clay galleries because of the increasing the polymer-sheet attractive interaction with the increase of polar groups amount, under the results of molecular dynamics simulations.[33]

Effect of the MAPP compatibilizer on the clay dispersion in PP/MAPP/C20A nanocomposites

In Figure 3(a), WAXD patterns of PP/MAPP/C20A nanocomposites with 3 wt % of clay prepared using different kinds of MAPPs as compatibilizers are presented. The interlayer spacing d_{001} values versus the compatibilizer MA content are shown in Figure 3(b) for PP/MAPP/C20A nanocomposites when compared with those of MAPP/C20A nanocomposites.

It is seen that in PP/MAPP/C20A nanocomposites the intercalation ability of MAPPs with 0.3–1.3% of MA is lower when compared with MAPP/C20A nanocomposites, apparently as a consequence of a

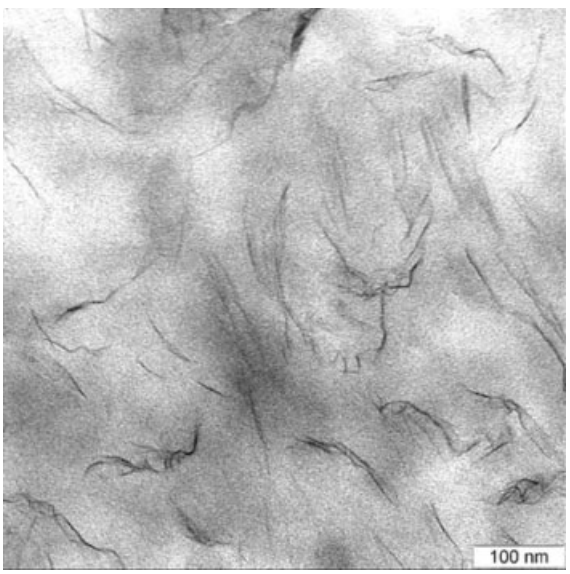

Figure 2 TEM image of MAPP1.3/C20A nanocomposite with exfoliated platelets.

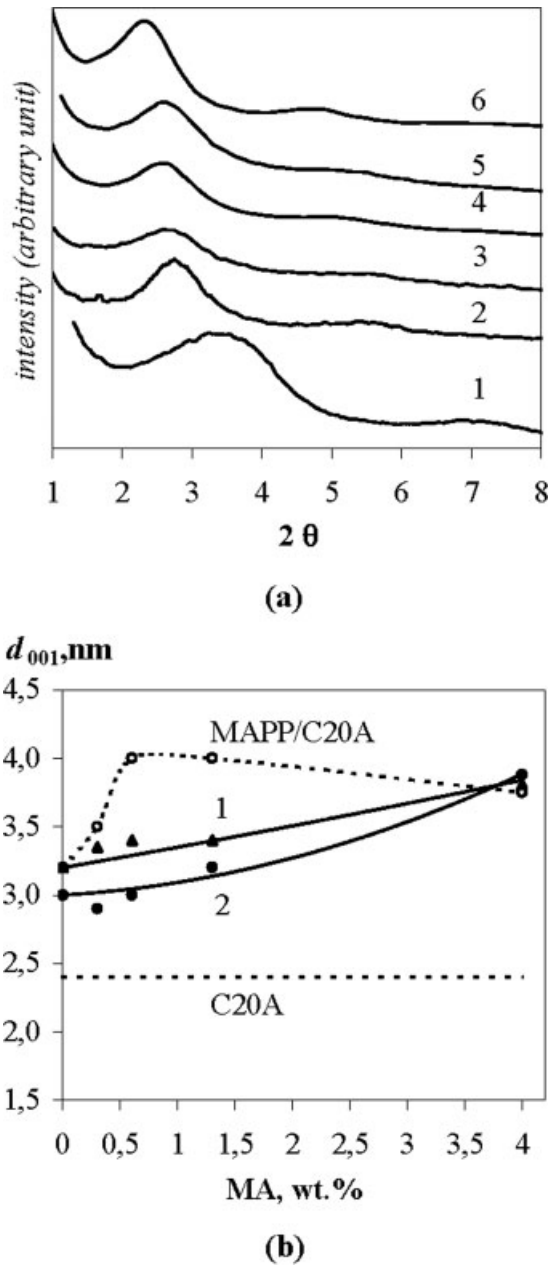

Figure 3 (a) WAXD patterns of organo clay C20A (1), composite PP/C20A without compatibilizer (2) and nanocomposite PP/MAPP0.3/C20A (3), PP/MAPP0.6/C20A (4), PP/MAPP1.3/C20A (5), and PP/MAPP4/C20A (6). C20A content is 3 wt %. (b) The dependencies of basal spacing d_{001} upon the MA content for the PP/MAPP/C20A nanocomposites with 3 (1) and 7 (2) wt % of C20A when compared with that of the MAPP/C20A nanocomposite with 3 wt % of C20A.

dilution of MAPP by nonpolar PP. With the increase in compatibilizer polarity, the d_{001} value rises and maximum one runs up to about 4 nm in the presence of oligomer MAPP4 with the highest MA content. With the increase in the C20A loading the tendency to decreasing interlayer spacing of clay is observed except for the nanocomposites compatibilized by highest polar MAPP4. Data obtained reveal that the ability of polymer to penetrate into the clay galleries in nanocomposites with polar compatibilizer rises with the increase in grafting content in the MAPP.

Along with the XRD technique, both TEM and AFM analyses were used for the purpose of the direct observation of the clay dispersion in the nanocomposites. Although the evident basal reflections related to the intercalated tactoids of clay are present at XRD diffractograms of composites with and without compatibilizer, TEM analysis showed an essential difference in their structures. Figure 4(a) shows the TEM micrograph for uncompatibilized PP/C20A system. The large aggregates of original particles as well as a few exfoliated plates can be seen. On the other hand, the compatibilized PP/MAPP4/C20A nanocomposite contains a higher number of exfoliated particles as well as the nanoscale clay tactoids [Fig. 4(b)]. At high magnification of TEM micrograph of PP/MAPP4/C20A nanocomposite [Fig. 4(c)], it is seen that the layered structure of intercalated tactoids is characterized by an essential inhomogeneous of the interlayer distances. In Figure 5, the AFM images of composites

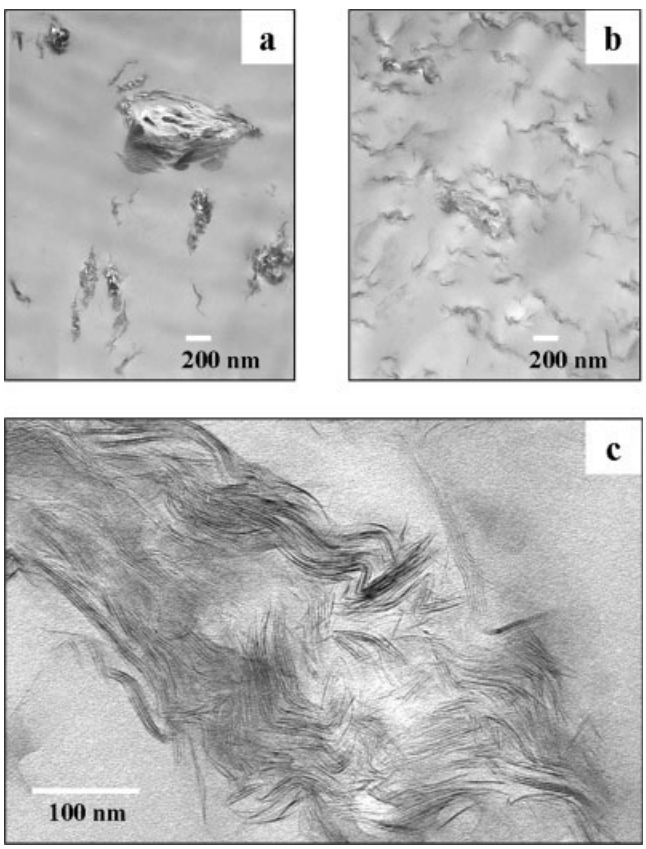

Figure 4 TEM images of PP/C20A composite without compatibilizer (a) and compatibilized PP/MAPP4/C20A nanocomposite (b, c). (c) High magnification. The C20A content is 7 wt %.

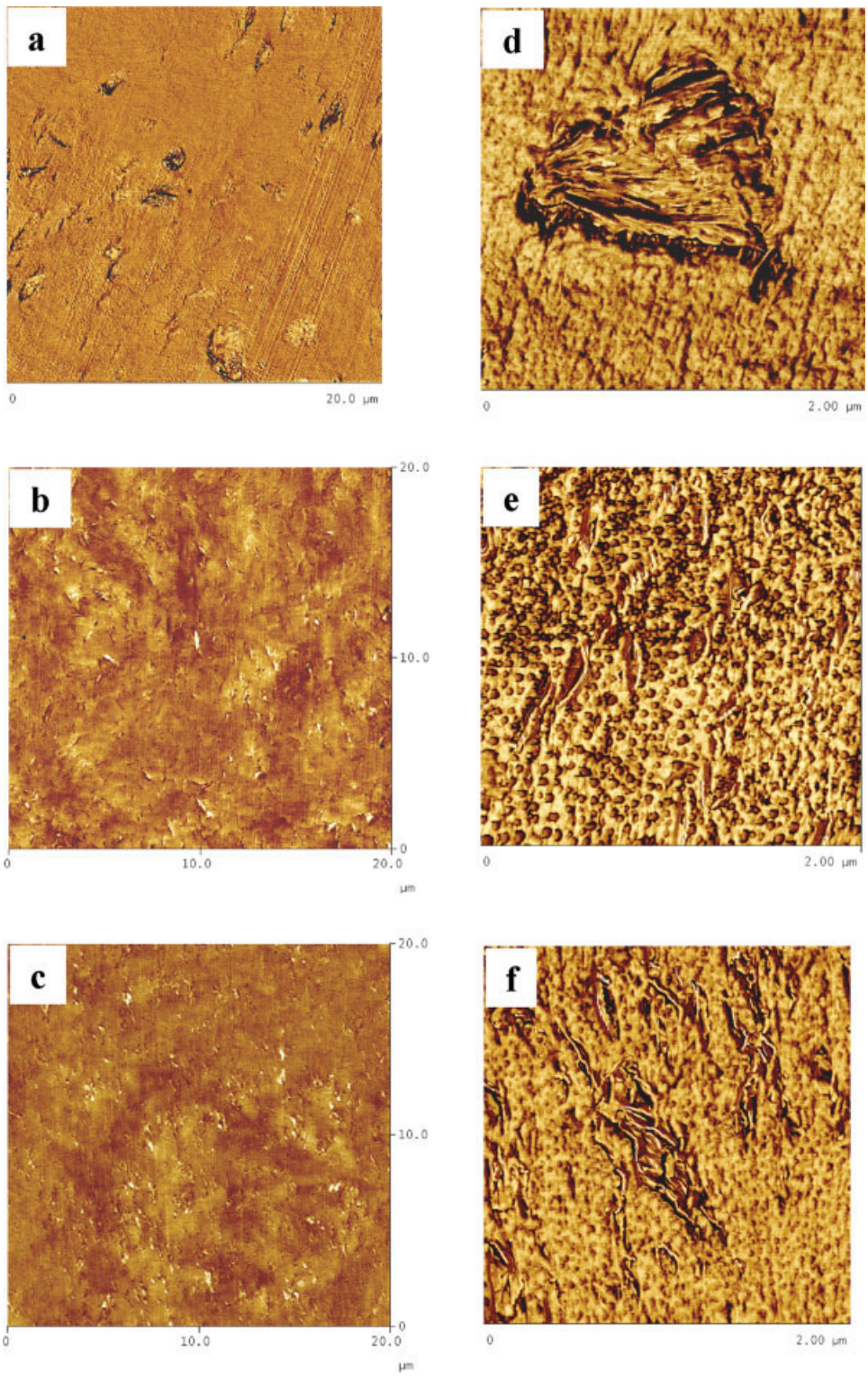

Figure 5 AFM images of composites without compatibilizer (a, d), with MAPP0.3 (b, e) and MAPP4 (c, f) at low (a–c) and high (d–f) magnifications. The C20A content is 7 wt %. [Color figure can be viewed in the online issue, which is available at www.interscience.wiley.com.]

without compatibilizer and with MAPP0.3 and MAPP4 are presented. The AFM analysis of the composite structures also confirmed that the polar compatibilizer essentially facilitates the dispersion and exfoliation of the layered silicate on nanosize tactoids and single-layered silicate platelets.

Thus, XRD, TEM, and AFM data revealed that the nanocomposites of the mixed intercalated/exfoliated

TABLE II
Thermal Characteristics of Neat Polymers, PP/MAPP Blends (80/20) and PP Nanocomposites

Sample	C20A (wt %)	T_m (°C) min	T_m (°C) shoulder	T_m (°C) max	ΔT_m (°C)	ΔH_m (J/g)	T_{cr} (°C)
PP	–	152		162	10	96	110
MAPP**0.3**	–	151	161	164	13	103	120
MAPP**0.6**	–	154	162	165	11	104	114
MAPP**1.3**	–	152.5	159	165	12	98	113
MAPP**4**	–	130	138	149	19	59	104
PP/MAPP**0.3**	–	153		162	9	100	113
PP/MAPP**0.6**	–	152.1		160	8	98	115
PP/MAPP**1.3**	–	150.9		160	9	98	113
PP/MAPP**4**	–	149.2		160	11	96	109
PP/C20A	7	155		164	9	98	112
PP/MAPP**0.3**/C20A	7	154		161.5	7.5	99	115
PP/MAPP**0.6**/C20A	7	152.7		163.4	10.7	93	113
PP/MAPP**1.3**/C20A	7	153.5		161	7.5	91	111
PP/MAPP**4**/C20A	7	149	158	163	14	89	111

morphology were formed in the presence of all used types of compatibilizers. However, the quantitative assessment of a fraction of exfoliated particles in the nanocomposites of mixed morphology remains an undecided problem for the present.

Melting and nonisothermal crystallization behavior of MAPPs, nonpolar/polar polymer blends and nanocomposites

The miscibility of the polymer compatibilizers with neat PP and the thermophysical properties of PP/MAPP blends and the composites were studied by DSC. DSC thermograms for melting (from 100 to 175°C) and crystallization (from 90 to 130°C) of original PP and MAPPs, PP/MAPP blends, and nanocomposites with 7 wt % of C20A are presented in Figures 6–8. Thermophysical characteristics of these materials are summarized in Table II.

A common feature for all maleated polymers is the clear bimodal fusion endotherms [Fig. 6(a)], unlike neat PP. The origin of the doublet in the melting peaks in the presence of functional groups in the side of the MAPP backbone molecules may be explained by their heterogeneous crystalline structure, namely by the presence of two populations of crystallites with different thermal stability.[34] As it is seen from Figure 6(b), the polar group content influences on the crystallization behavior of the MAPPs essentially. For MAPP0.3, the T_{cr} increases to 120°C compared with $T_{cr,PP}$ = 110°C. It means that the low amount of polar groups can promote a nucleating activity during the polymer crystallization, resulting in moderate increase in both the melting temperature T_m and heat of fusion ΔH_m (Table II). On the contrary for MAPP with 4 wt % of the MA groups the T_{cr} drops to 104°C, hence the high grafting content in the polymer chains makes difficult their crystallization and as a result imperfect crystals with low T_M form. Really, the high polar oligomer MAPP4 has the clearly defined bimodal endotherm and the broadest melting range with the melting peak at 148°C and the low temperature shoulder about 138°C, compared with T_m = 162°C for the neat PP. Moreover, the onset melting temperature and ΔH_m decrease also indicate the deterioration of thermal properties of the high polar maleated polymer as a result of its imperfect crystalline structure (Table II).

Both the PP/MAPP blends [Fig. 7(a)] and the compatibilized nanocomposites PP/MAPP/C20A [Fig. 8(a)] demonstrate the single fusion endotherms. Marked trend to closing in the T_{cr} values [Figs. 7(b) and 8(b)] and the absence of double melting peak indicate that the cocrystallization of polar MAPPs with the PP takes place at used cooling conditions. In Figure 9, the dependencies of T_{cr} and ΔH_m upon the MAPP grafting content are plotted for both PP/MAPP blends and nanocomposites with 7 wt % of the clay. The PP/MAPP blends have rather higher T_{cr} and crystallinity compared with those of the neat PP except for MAPP with 4% of the MA (Table II, Fig. 9). The high polar and low MW MAPP4 has limited miscibility with PP and as a result the imperfect crystal fraction with deteriorated thermal properties forms. The clay particles exhibit the weak nucleation effect manifested in a slight increasing the T_{cr} for the binary PP/C20A composite compared with that of the neat PP as well as for the nanocomposites modified by the

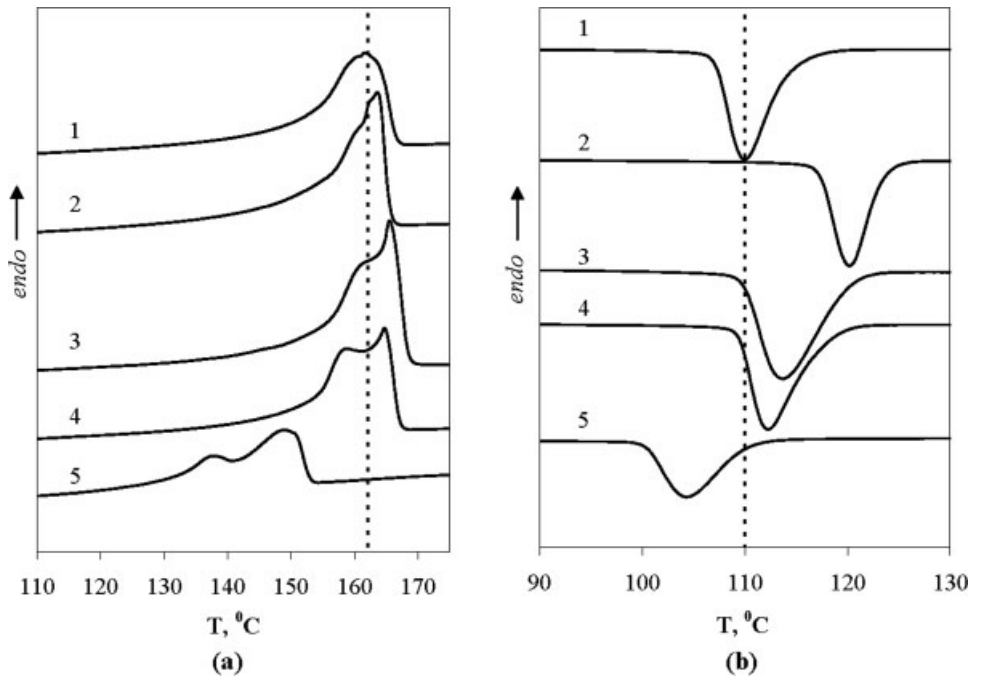

Figure 6 DSC melting (a) and crystallization (b) curves for neat PP (1), MAPP0.3 (2), MAPP0.6 (3), MAPP1.3 (4), and MAPP4 (5).

low MW MAPP0.3 and MAPP4 compatibilizers compared with the T_{cr} of the appropriate matrix blends. All the same distinguishing features of the nanocomposite based on PP/MAPP4 matrix are the lowest T_{cr} and the most asymmetric shape of the melting endotherm characterized by lowest onset melting temperature and the most heterogeneous distribution of the crystallite sizes [Table II, Fig. 8(a), curve 6].

Thus the results obtained reveal a complicated role of the chemical structure of the maleated PP as compatibilizer in the melt mixing of the PP with organoclay. The low MW MAPP0.3 with the low grafting

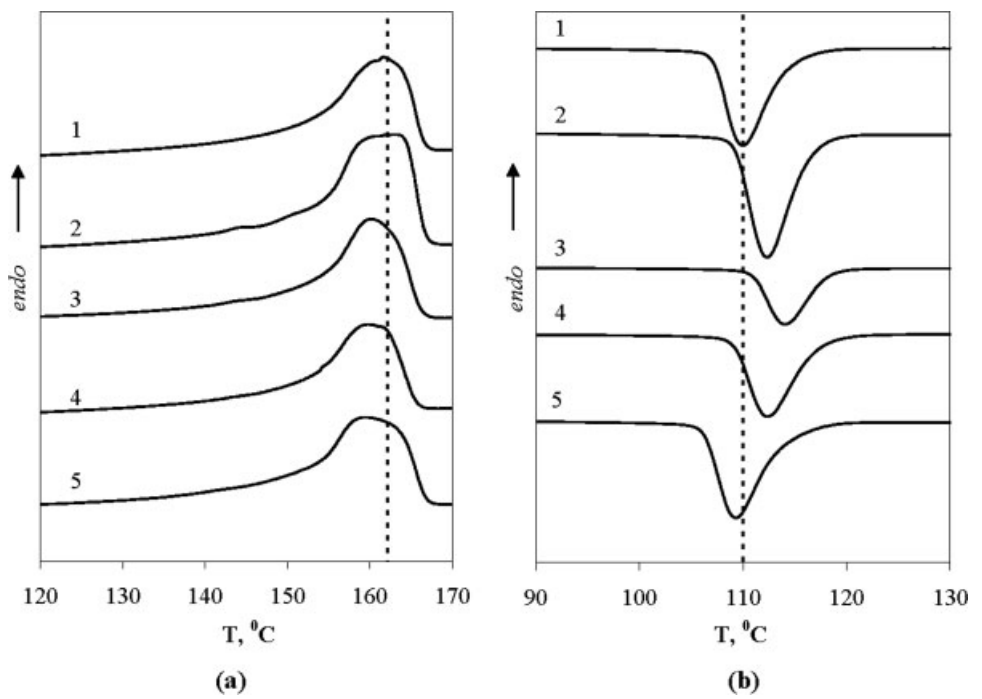

Figure 7 DSC melting (a) and crystallization (b) curves for neat PP (1) and polymer blends: PP/MAPP0.3 (2), PP/MAPP0.6 (3), PP/MAPP1.3 (4), and PP/MAPP4 (5). PP/MAPP = 80/20.

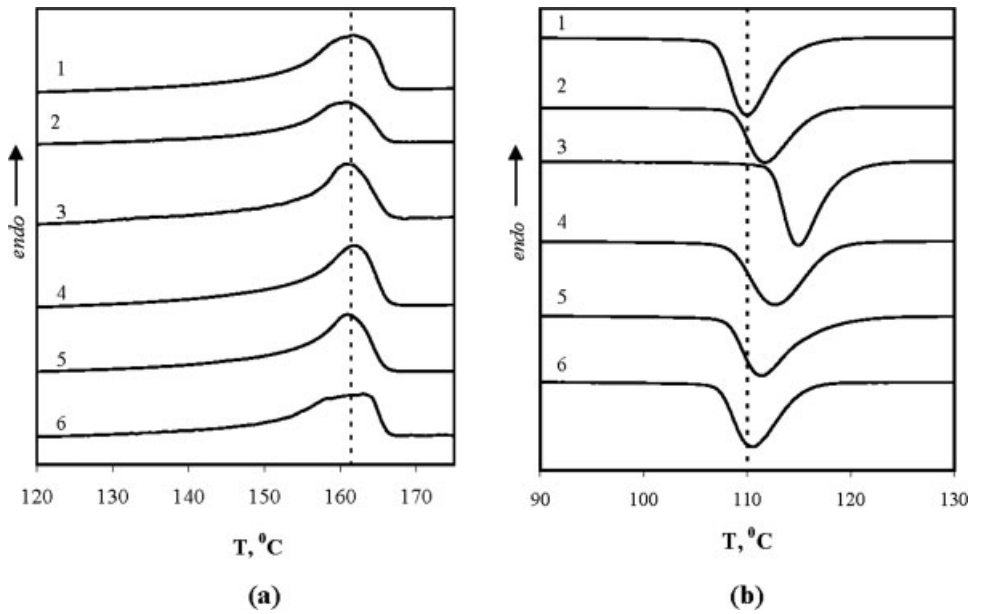

Figure 8 DSC melting (a) and crystallization (b) curves for neat PP (1) and nanocomposites with 7 wt % of C20A: PP/C20A (2), PP/MAPP0.3/C20A (3), PP/MAPP0.6/C20A (4), PP/MAPP1.3/C20A (5), and PP/MAPP4/C20A (6).

content shows the low intercalation capability but leads to the increase in the crystallinity of nanocomposite polymer matrix. The increase in the MA content in the compatibilizer leads simultaneously to the increase of intercalation level (the clay interlayer spacing increases from 2.4 to 4 nm) (Fig. 3) and to the decrease in the crystallinity of nanocomposite polymer matrix. As the last effect was observed neither in PP/MAPP nor in PP/clay binary composites, the decrease in the polymer matrix crystallinity in nanocomposites simultaneously with the increase in the intercalation level may be qualitative indicator of the difficult crystallization of confined polymer chains between the clay platelets.

Tensile properties and impact toughness

The tensile properties of the neat PP and MAPPs, the PP/MAPP blends with 20 wt % of MAPP and the composites without and with compatibilizers are listed in Table III. The 20 wt % of MAPP in polymer blends is in keeping with the compatibilizer content in the nanocomposites with 7 wt% of C20A and MAPP/C20A = 3:1. It can be seen that the elastic moduli and yield stresses of MAPPs are higher when compared with those of PP. The maleated polymers fracture in the brittle manner. The smaller modulus and slight ability to plastic deformation are characteristic just for the high MW MAPP0.6. The introduction of MAPP into the PP matrix changes its mechanical properties, particularly, the elastic moduli and yield stresses of blends increase somewhat whereas the ultimate elongations decrease. The deformation properties of PP/MAPP blends drop most sharply in the presence of oligomer MAPP4. Hereinafter, the tensile properties of compatibilized composites were compared with those of both neat PP and the PP/MAPP blends.

In Figure 10, the relative moduli (E/E_{PP}) of nanocomposites with 3 and 7 wt % of clay are plotted as

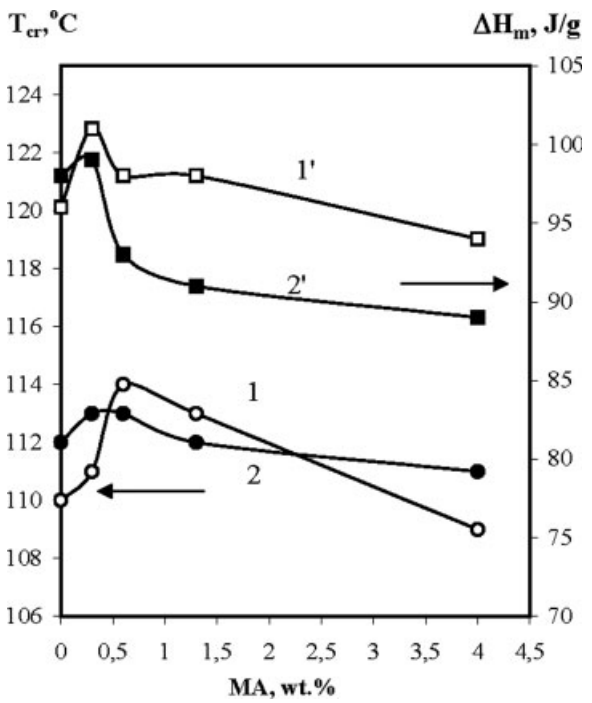

Figure 9 The dependencies of T_{cr} (1, 2) and ΔH_m (1′, 2′) upon the compatibilizer grafting content for PP/MAPP blends (1, 1′) and nanocomposites with 7 wt % of the clay (2, 2′).

TABLE III
The Tensile Properties and Impact Strengths of Neat PP, PP/MAPP Blends (80/20) and PP Nanocomposites

Samples	Clay wt %	Clay vol %	MFI_{MAPP} (g/10 min)	MAPP (wt %)	Young's modulus (MPa)	Yield stress (MPa)	Yield strain (%)	Tensile strength (MPa)	Elongation at break (%)	Impact toughness (kJ/m^2)
PP	–	–	0,6	–	1083 ± 110	33.0 ± 0.2	13.2 ± 0.3	49.0 ± 0.7	1050 ± 120	4.7 ± 0.6
MAPP**0.3**	–	–	162	100	1820 ± 180	[a]	[a]	40.0 ± 0.5	7 ± 0.2	–
MAPP**0.6**	–	–	12	100	1476 ± 148	38.0 ± 0.4	9.2 ± 0.3	31.5 ± 1	26 ± 8	–
MAPP**1.3**	–	–	43	100	1501 ± 65	[a]	[a]	40.0 ± 0.5	8 ± 1	–
MAPP**4**	–	–	Wax	100	[b]	[b]	[b]	[b]	[b]	–
PP/MAPP**0.3**	–	–		20	1380 ± 97	37.0 ± 0.2	10.8 ± 0.3	41.7 ± 4.3	734 ± 144	
PP/MAPP**0.6**	–	–		20	1183 ± 170	36.0 ± 0.4	11.2 ± 0.1	48.2 ± 1.2	911 ± 35	–
PP/MAPP**1.3**	–	–		20	1312 ± 40	36.0 ± 0.7	11.2 ± 0.1	39 ± 4	722 ± 147	–
PP/MAPP**4**	–	–		20	1172 ± 74	33.7 ± 0.3	11.1 ± 0.3	30.4 ± 1.3	556 ± 66	–
PP/C20A	3	1.6		–	1298 ± 26	35.4 ± 0.4	11.2 ± 0,8	50.0 ± 1.5	897 ± 23	4.7 ± 0.5
	7	3.8		–	1500 ± 80	36.9 ± 0.5	9,4	33	500 ± 100	4.85 ± 0.5
PP/MAPP**0.3**/C20A	3	1.6		9	1400 ± 80	35.0 ± 0.2	10.4 ± 0.5	42 ± 4	774 ± 110	3.7 ± 0.3
	7	3.8		21	1563 ± 105	34.9 ± 0.4	7.0 ± 0.2	24.7 ± 4	1.5 ± 2.6	2.3 ± 0.3
PP/MAPP**0.6**/C20A	3	1.6		9	1519 ± 170	36.0 ± 0.5	10.4 ± 0.3	42.6 ± 7.2	748 ± 191	5.0 ± 0.2
	7	3.8		21	1791 ± 80	37.0 ± 0.6	7.4 ± 0.5	29 ± 3	253 ± 60	3.9 ± 0.6
P/MAPP**1.3**/C20A	3	1.6		9	1350 ± 55	34.2 ± 0.3	9.7 ± 0.2	42 ± 3	777 ± 120	4.8 ± 0.8
	7	3.8		21	1599 ± 150	35.6 ± 0.4	7.7 ± 0.2	26.8 ± 0.4	60 ± 6	3.2 ± 0.5
PP/MAPP**4**/C20A	3	1.6		9	1266 ± 50	35.6 ± 0.3	9.8 ± 0.2	25.5 ± 3.8	480 ± 88	3.7 ± 0.4
	7	3.8		21	1484 ± 77	[a]	[a]	32.7 ± 3.2	6.5 ± 0.3	1.7 ± 0.2

[a] Brittle fracture.
[b] It is impossible to cut a specimen for tensile test because a brittleness of material.

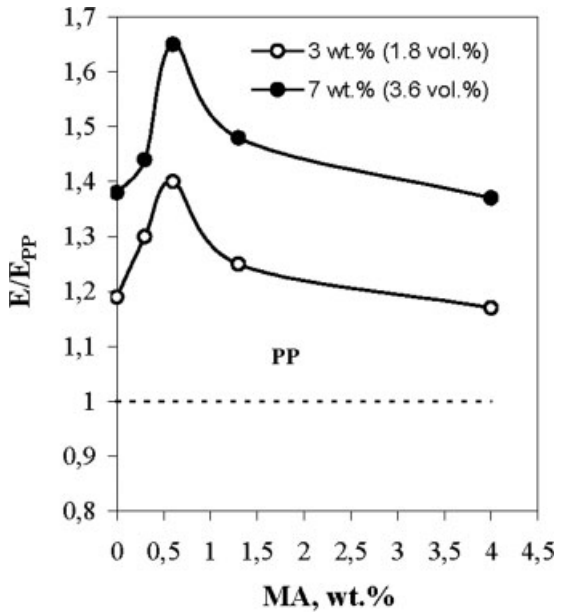

Figure 10 The relative moduli E/E_{PP} of nanocomposites with 3 and 7 wt % of clay as functions of the compatibilizer grafting content.

the function of the compatibilizer grafting content. The E/E_{PP} values become higher as the clay content increases. The dependencies of reinforcing effect E/E_{PP} of clay upon the MA content have extreme character for both clay volumes. Maximum reinforcing effect is attained using high MW MAPP with 0.6% MA. The elastic modulus of such nanocomposite with 7 wt % (3.8 vol %) of clay is almost 1.7 times higher when compared with that of neat PP and 1.3 times higher when compared with that of nonmaleated nanocomposites. To understand the role of hybrid matrix stiffness, we attempted to arrange the experimental data on the nanocomposite moduli in order increasing the PP/MAPP blend moduli, and it turned out that this order coincides with the increasing melt index of compatibilizer (decreasing its MW) (Table I) except for the blend with oligomer MAPP4. In Figure 11(a), the modulus enhancement levels relative to neat PP (E/E_{PP}) are confronted for both PP/MAPP blends and nanocomposites. In Figure 11(b), the modulus enhancement for nanocomposites relative to corresponding matrices (E/E_{matrix}) is shown. As can be seen, there is no correlation between the increase in hybrid matrix stiffness and the enhancement of the elastic moduli of compatibilized nanocomposites [Fig. 11(a)]. The PP/MAPP0.6 blend shows a least increase in the elastic modulus when compared with that of PP; at that in the nanocomposites based on the PP/MAPP0.6 hybrid matrix, the most reinforcing effect of layered silicate E/E_{PP} is achieved. The comparison of the nanocomposite moduli relative to those of hybrid matrices also revealed the most reinforcing effect E/E_{matrix} for the nanocomposites PP/MAPP0.6/C20A [Fig. 11(b)]. Evidently, the most effectiveness of MAPP0.6 as compatibilizer can be caused by better miscibility with PP because higher MW and moderate grafting content as well as by some higher level of exfoliation of the intercalated clay tactoids compared with MAPPs with lower MW and higher polarity.

The yield stresses of the nanocomposites are slightly higher than that of neat PP indicating a high interfacial interaction between the polymer matrix and clay (Table III). Also, the SEM observations of deformed specimens did not show evident voiding in the zone of a transition to the neck [Fig. 12(a)]. In the neck area during plastic flow, debonding of particles occurs followed by the accumulation of voids [Fig. 12(b)]. The study of deformation mechanism in PP/clay nanocomposites in Ref. 35 also revealed debonding the clay particles during necking.

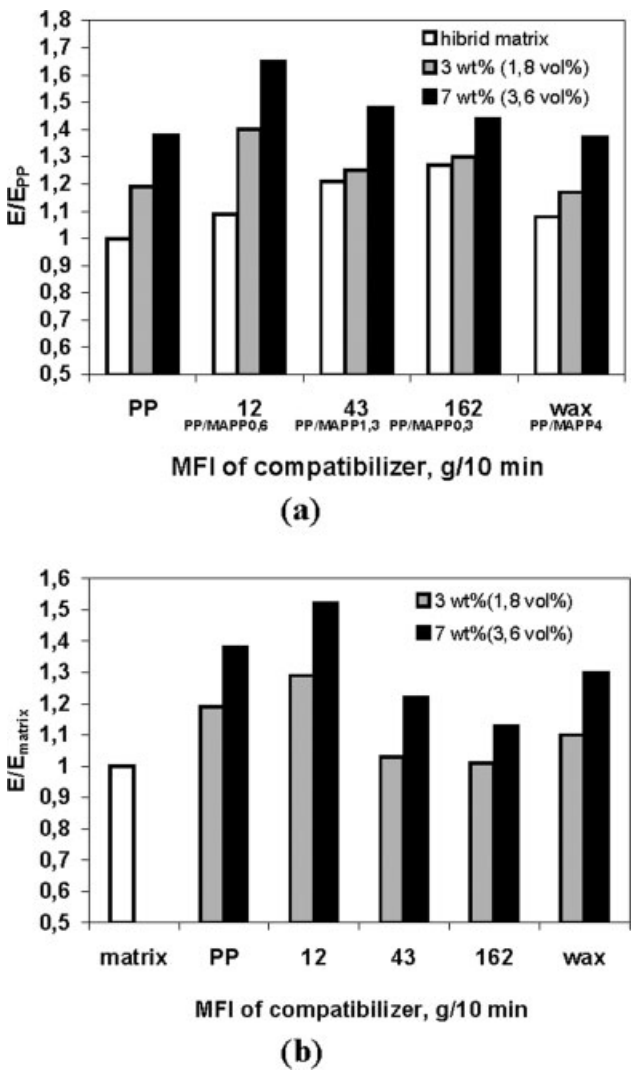

Figure 11 (a) The moduli of PP/MAPP blends and nanocomposites with 3 and 7 wt % of clay, relative to neat PP (E/E_{PP}) and (b) moduli of nanocomposites relative to corresponding matrix (E/E_{matrix}) as function of the compatibilizer MFI (or molecular weight).

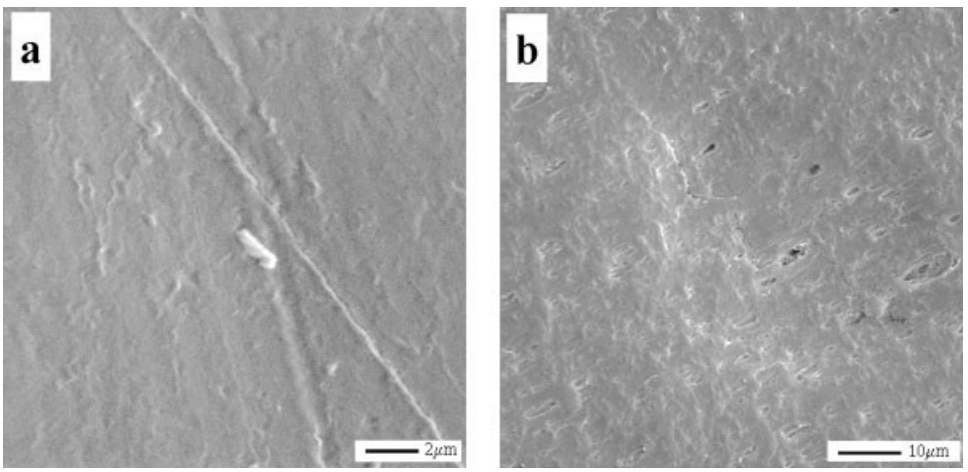

Figure 12 SEM micrographs of tensile deformed specimen PP/MAPP0.6/C20A with 7 wt % of clay: the zone before the neck area without voids (a), debonding of clay particles in the neck area (b).

The elongation at break of the PP slightly decreases in the presence of the maleated polymers to a greater extent in the case of MAPP0.3 and MAPP4 with low MW or high content of polar groups (Table III, Fig. 13). The introduction of 3 wt % of clay lightly reduces the nanocomposite deformation properties compared with those of corresponding PP/MAPP blends. When the clay content increases still more, some ability to a plastic flow keeps only for the composites without MAPP and with MAPP0.6, whereas the nanocomposites containing low MW MAPPs (with both 0.3 and 4% of MA) exhibit brittle fracture. The analysis of a ratio between the fracture and yield stresses revealed that the strainhardening decreases most of all in the presence of MAPP4 for both the PP/MAPP4 blend and PP/MAPP4/C20A nanocomposite (Table III). Apparently, the drop of the fracture strengths of nanocomposites modified by MAPP4 and MAPP0.3 causes also the more drastic drop of their impact toughness, whereas the toughness of the nanocomposites with higher MW compatibilizers (MAPP0.6 and MAPP1.3) keeps to a greater extent (Table III).

The data obtained show that the MAPP0.6 have the most optimal structure parameters (both grafting content and MW) among the used compatibilizers from the point of view of the reinforcing effect of layered silicate, the deformation properties, and impact toughness of nanocomposites.

In Figure 14, the effect of filler content on the relative elastic moduli of PP composites is compared with the PP/MAPP/C20A nanocomposites studied and the PP/glass beads (with d_{GB} = 3 μm) microcomposites.[36] It is seen that the same reinforcing effect of rigid filler can be achieved by the introduction of ei-

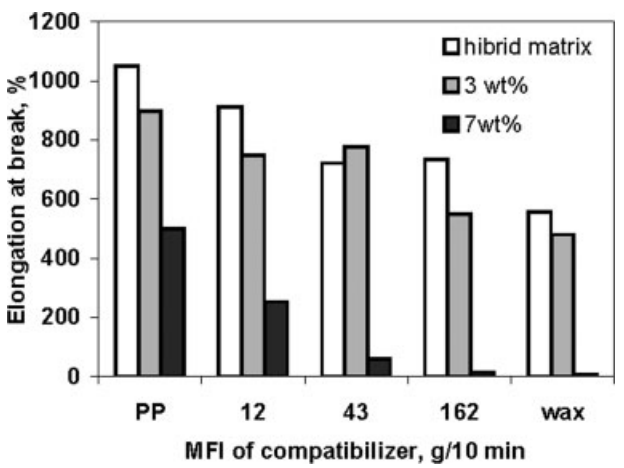

Figure 13 The elongation at break for PP/MAPP blends and nanocomposites with 3 and 7 wt % of clay as function of the compatibilizer melt index.

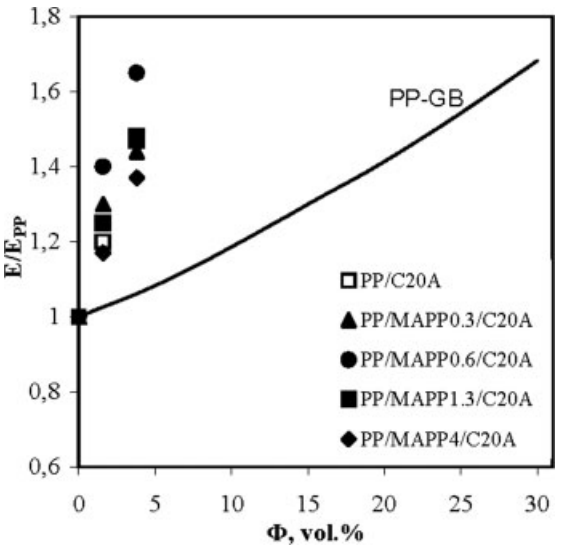

Figure 14 The relative elastic moduli for the PP/MAPP/C20A nanocomposites and conventional PP/glass beads (with d = 3 μm) microcomposites as function of filler content.

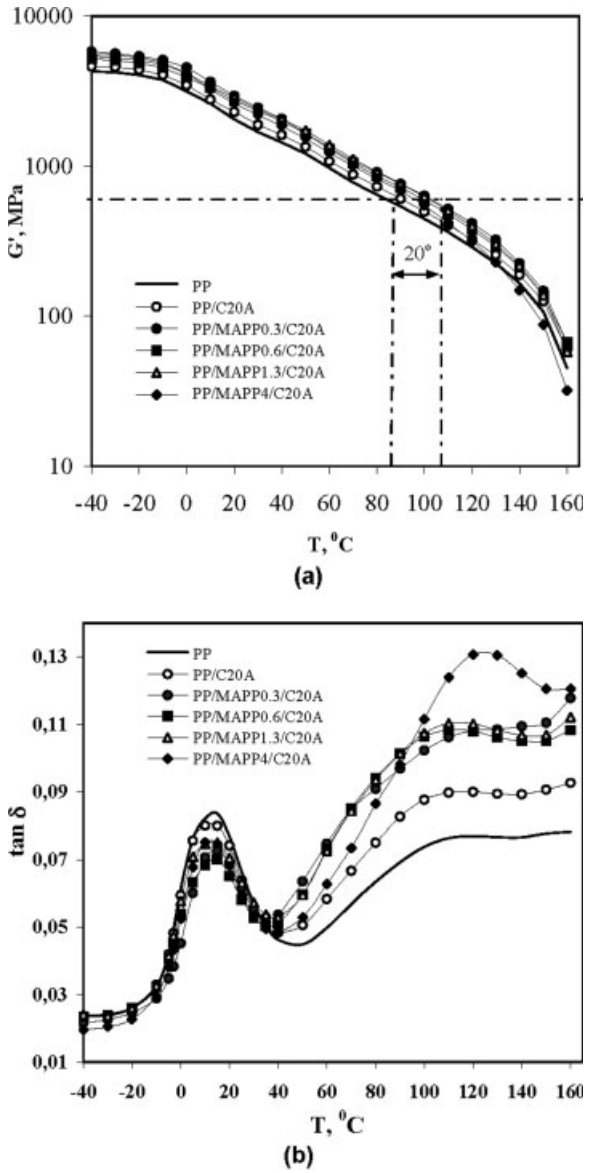

Figure 15 Dependencies of the dynamic storage moduli (a) and tan δ (b) upon temperature for the neat PP and nanocomposites containing 7 wt % of clay without and with compatibilizers.

ther about 4 vol % of layered silicate or 20–30 vol % of microscale filler with spherical particle.

Dynamic mechanical properties of nanocomposites depending on compatibilizer types

To investigate the reinforcing effect of layered silicate in a broader temperature range, dynamic mechanical analysis (DMA) of nanocomposites has been carried out at a fixed frequency of 10 Hz in the temperature range of −40 to 160°C. In Figure 15, the temperature dependencies of the dynamic storage moduli G' (a) and loss factor tan δ (b) are shown for the neat PP and nanocomposites containing 7 wt % of clay with and without compatibilizers. As can be seen from Figure 15(a) the dynamic storage moduli of modified nanocomposites are higher when compared with that of nonmodified composite. The systems containing the MAPPs with the MA groups in the range of 0.3–1.3 wt % exibit very similar trends in the modulus–temperature curves at all temperatures, whereas the oligomer MAPP with 4 wt % of polar groups makes for decreasing composite G' above 80°C. This effect is seen more clearly in Figure 16, where the relative dynamic moduli G'/G'_{PP} of above nanocomposites are shown as the functions of both temperature and MAPP type. The temperature dependencies of tan δ for PP and PP/clay nanocomposites with 7 wt % of clay show two relaxation peaks: one at 14°C and another slight degraded peak between 50 and 140°C [Fig. 15(b)]. The dominant relaxation at ~ 14°C is the glass–rubber relaxation of the amorphous phase of PP. The second high temperature wide peak on tan δ–T curve is observed frequently for the semicrystalline polymers[2,37,38] and is associated with the phenomena such as intracrystalline relaxation (α- relaxation) and sliding of tied chains within crystalline blocks of PP. The presence of clay particles does not influence on the glass transition temperature (T_g) of PP. The intensity of low temperature relaxation peak slightly decreases for the modified composites; at the same time, the intensity of high temperature peak rises gradually with the introduction of clay and compatibilizers.

Below T_g, the relative storage moduli of nanocomposites are 1.2–1.3 to that of PP; above T_g, the moduli increase up to 1.4–1.5 at around 30–75°C and then

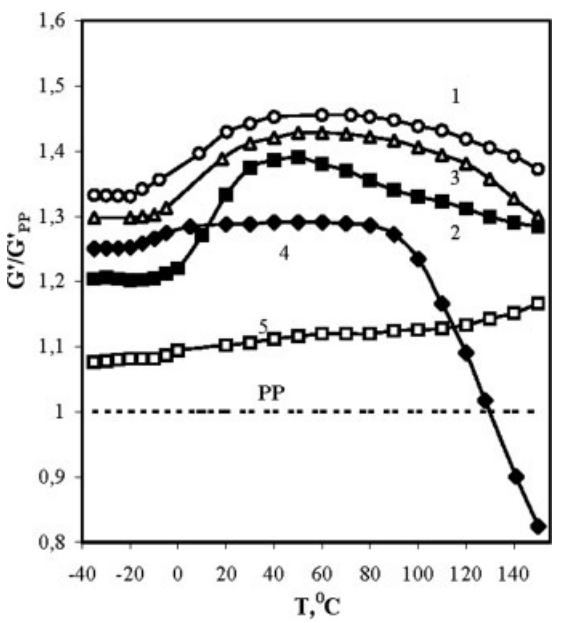

Figure 16 Temperature dependencies of the relative dynamic storage moduli G'/G'_{PP} for nanocomposites without and with compatibilizer. The C20A content is 7 wt %.

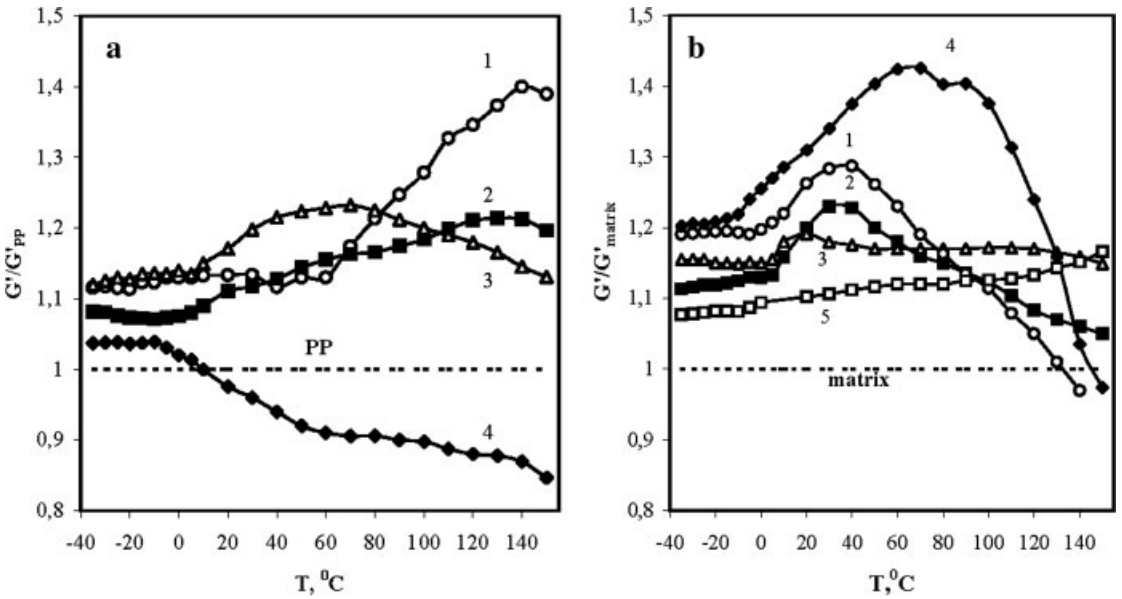

Figure 17 Temperature dependencies of the relative storage moduli G'/G'_{PP} of the PP/MAPP blends (a) and the relative storage moduli G'/G'_{matrix} of the nanocomposites (b) with MAPP0.3 (1), MAPP0.6 (2), MAPP1.3 (3), MAPP4 (4), and without compatibilizer (5).

slightly decrease to melt (Fig. 16). Substantial distinction of the nanocomposite with oligomer MAPP4 becomes apparent as a sharp drop of the G' above 80°C and decrease of modulus compared with those of uncompatibilized composite and PP, correspondingly, above 120 and 130°C. Similar effect of high polar oligomer compatibilizer on the dynamic modulus of the PP/clay nanocomposites was reported in Refs. 24 and 39. In the nanocomposite with oligomer MAPP4, most increasing intensity of high temperatureα-relaxation peak takes place [Fig. 15(b)].

To clarify an effect of the MAPP type on the temperature behavior of hibryd polymer matrices, the relative dynamic storage moduli G'/G'_{PP} for the PP/MAPP blends [Fig. 17(a)] and the relative moduli G'/G'_{matrix} for the nanocomposites (to those of corresponding polymer matrices) [Fig. 17(b)] were plotted as functions of both temperature and MAPP type. As can be seen from Figure 17(a), above T_g tendency to the increase of storage moduli compared with neat PP is observed for the blends containing the MAPPs with the MA groups in the range of 0.3–1.3 wt %. This effect is highest for MAPP0.3 and decreases when grafting content in MAPP increases. In contrast, the G' value of PP/MAPP4 blend becomes lower compared with that of neat PP, already about 0°C, because of limited miscibility of oligomer high polar MAPP4 with PP and more imperfect crystalline structure of the hybrid polymer matrix (Table II). This data show that the decrease in thermal–mechanical stability of PP/MAPP4/C20A nanocomposite compared with PP [Fig. 16(a)] can be attributed to lower thermal–mechanical stability of the hybrid polymer matrix PP/MAPP4 compared with that of neat PP.

At the same time, the relative storage moduli G'/G'_{matrix} of nanocomposite with MAPP4 are highest compared to those of the nanocomposites with other compatibilizers [Fig. 17(b)]. It is interesting that in PP/MAPP4/C20A nanocomposite the α-relaxation peak maximum shifts distinctly to a high temperature area (about 15°C) compared to both neat PP and other compatibilized nanocomposites [Fig. 15(b)]. Such effect is the characteristic feature for intercalated PP/MAPP4/C20A nanocomposites with both 3 and 7 wt % of clay and is observed neither in the PP/MAPP4 blend nor in the PP/C20A binary composite (Fig. 18).

Simultaneity of the shift of α-relaxation peak maximum to a high temperature area for PP/MAPP4/C20A nanocomposites [Figs. 15(b) and 18] as well as the strong enhancement of the storage moduli of PP/MAPP4/C20A nanocomposite in relation to those of the PP/MAPP hybrid matrix [Fig. 17(b)] can be caused by the increase in a content of the intercalated polymer [Fig. 3(b)] and fraction of ''rigid'' amorphous phase (Fig. 9) with lower mobility of the polymer chains confined within interlayer space as well as high adhesion between the polar MAPP4 and clay platelets surface. However, an additional study of the effects of the intercalated polymer structure and compatibilizer mechanical properties on the nanocomposite mechanical behavior is necessary.

The results obtained clearly show that at the use of the polar polymer compatibilizers the problem of a competition between intercalation ability and misci-

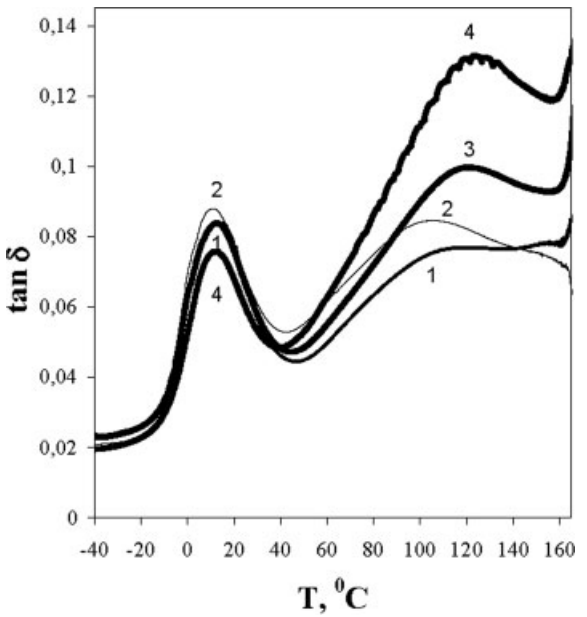

Figure 18 Temperature dependencies of the tan δ for the neat PP (1), PP/MAPP4 blend (2), and nanocomposites PP/MAPP4/C20A with 3 (3) and 7 wt % (4) of clay.

bility of polymers exists. The compatibilizer with both high MW and optimal polar group content (~ 0.6 wt % of grafting content) ensures the remarkable reinforcing effect of layered silicate without loss of impact toughness (Table III) and improves of the thermal–mechanical stability of PP/MAPP/clay nanocomposites at high temperature [Fig. 16(a)]. On the other hand, the oligomer MAPP with the high polar group content is inefficient in respect to preservation of the nanocomposite stiffness at high temperature and leads to sharp drop of the material toughness.

Flammability properties of PP-based nanocomposites

A large number of traditional flame retardants (FRs) are used for PP in industry applications: halogenated FR, phosphorous-containing FR, and magnesium hydroxide (MH).[40] Today, MH is the commercially prevalent and ecologically friendly FR for PP. In the last years, the modern approach to the enhancement of thermal stability and fire resistance of the polyolefin materials based on the use of polymer nanocomposites has been extensively developed.[40–47] Recently, the study of FR properties of PP/layered silicate nanocomposites showed the loading of only 4–7 wt % of clay to the PP yields in more than 100% decrease of the maximum heat release rate (HRR).[48–50]

The flammability characteristics of neat PP, PP/MAPP4/C20A nanocomposite with 7 wt % of clay and PP/MH composite with 60 wt % of MH were examined with a cone calorimeter at an external heat flux of 35 kW/m^2. The dependencies of the HRR versus time for those materials are presented in Figure 19(a). It is seen that the maximum HRR for PP is 2060 kW/m^2 (curve 1), for nanocomposite PP/MAPP4/C20A it is 844 kW/m^2 (curve 2), and for PP/MH composite with 60 wt % of MH it is 310 kW/m^2 (curve 4). Correspondingly, the HRR peaks for the composites containing either C20A or MH decrease by factors greater than two and six. The effect of twofold reduction in the maximum rate of heat release in polymer/clay nanocomposite may be explained in terms of the formation of a protective char layer on the burning polymer surface [Fig. 19(b)]. The mechanism of action of MH is based on the dilution of gaseous flame zone by the water vapor and its endothermic effect in solid phase.

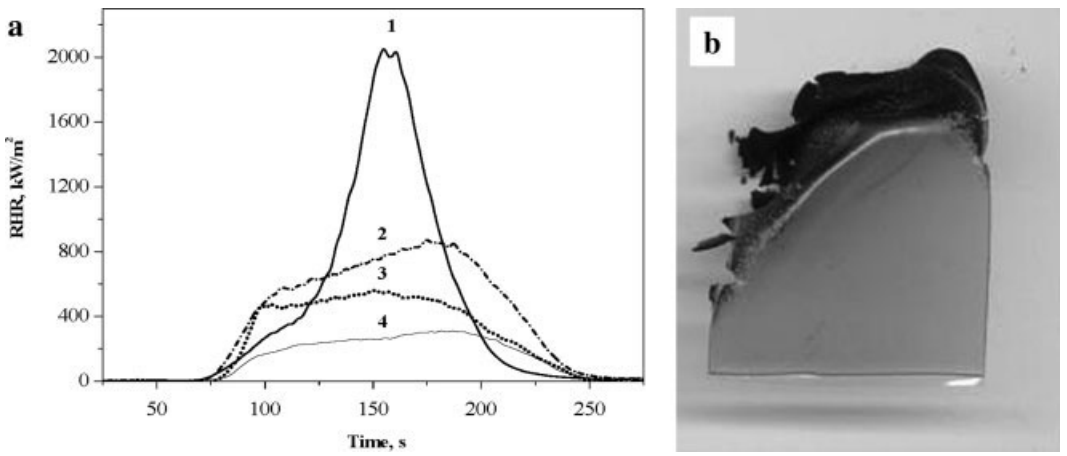

Figure 19 (a) Plot of the heat release rate versus time for neat PP (1), nanocomposite PP/MAPP4/C20A with 7 wt % of clay (2), complex nanocomposite of PP/MAPP4/C20A/MH with both 6wt % of clay and 20 wt % of MH (3), and composite PP/MH with 60 wt % of magnesium hydroxide (4) as measured in cone calorimeter tests. (b) The image of char-like residue of burnt PP nanocomposite specimen.

In the same figure, the dependency of the HRR versus time is also shown for the complex composite PP/MAPP4/C20A/MH containing 6 wt % of C20A and 20 wt % of MH (curve 3). As it can be seen, the addition of 20 wt % of MH to PP/MAPP4/C20A nanocomposite lowers the maximum HRR from 844 to 520 kW/m^2, i.e., by factors of four compared to neat PP. Thus, the creating complex composites including both the layered silicate and relatively small amount of MH can be a successful approach to improve the flammability properties of PP-based materials.

CONCLUSIONS

The effect of the type of MAPP as polar compatibilizer on the clay dispersion, its miscibility with polymer matrix, and properties of PP/layered silicate (C20A) nanocomposites was studied. Four types of MAPPs in broad range of grafting content (0.3–4 wt %) and MWs were used. The series of composites based on various combinations of neat PP, MAPP, and organoclay were prepared by melt compounding in Brabender mixer. The clay loadings were 3 and 7 wt %. In nanocomposites based on MAPP matrices, the intercalation capability of polymer into interlayer galleries runs up to maximum for MA content of 1.3 wt %: the interlayer spacing expands from 2.4 nm for C20A at most up to 4 nm and the most fractions of exfoliated single-layered silicate platelets forms. TEM and AFM analyses of uncompatibilized PP/C20A system showed the large aggregates of particles with a relatively limited intercalation. In the presence of all studied compatibilizers, the nanocomposites of mixed intercalated/exfoliated morphology are formed. It was found the morphology and properties of compatibilized PP/layered silicate nanocomposites are determined by polar groups content and the MW of the compatibilizer. The oligomer MAPP with 4 wt % of polar groups increases the intercalation ability of polymer but this one has limited miscibility with PP and worsens the polymer crystalline structure. The MAPPs with 0.3–1.3% of MA are cocrystallized with PP well. The highest reinforcing effect of clay as well as the ability of nanocomposite to a plastic flow and preservation of impact toughness was observed in the presence of high molecular compatibilizers with 0.6–1.3% of MA. Dynamic storage moduli of such nanocomposites with 7 wt % of clay increase up to 1.4–1.5 around 30–75°C and over the whole temperature range remain higher compared with both the neat PP and uncompatibilized composites. The oligomer MAPP with 4 wt % of MA groups decreases thermal–mechanical stability of both the polymer blend and nanocomposites when compared with PP. Thus, high polar oligomer compatibilizer increases the intercalation ability of the polymer into the interlayer galleries of clay but it is inefficient from the point of view of improving material stiffness at high temperature because its limited miscibility with the nonpolar matrix polymer. The data obtained showed that the MAPP0.6 has the most optimal parameters (grafting content and MW) among the used compatibilizers from the viewpoint of the intercalation capability, polymer–clay adhesion, and miscibility with polymer matrix. The study of the nanocomposite flammability properties showed the creation of complex composites containing both layered silicate and relatively small amount of MH can be a successful approach to reduce the combustibility of PP-based materials.

Authors thank Clariant GmbH Co. for their kind supply of Licomont AR 504, Uniroyal Chemical Co. Inc, Crompton Co., for their kind supply of Polybond 3002 and Polybond 3150, Dr. N. A. Erina (Veeco Metrology of LLC AFMs, Santa Barbara) for the AFM analysis of the composites, and Dr. A. N. Shchegolikhin (Emmanuel Institute of Biochemical Physics, Russian Academy of Sciences) for the DSC analysis of the specimens.

References

1. Alexandre, M.; Dubois, P. Mater Sci Eng 2000, 28, 1.
2. Ray, S. S.; Okamoto, M. Prog Polym Sci 2003, 28, 1539.
3. Usuki, A.; Hasegawa, N.; Kato, M. Adv Polym Sci 2005, 179, 135.
4. Bridley, S. W.; Brown, G. Crystal Structure of Clay Minerals and Their X-Ray Diffraction; Mineralogical Society: London, 1980.
5. Pinnavaia, T. J. Science 1983, 220, 365.
6. Vaia, R. A.; Giannelis, E. P. Macromolecules 1997, 30, 7990.
7. Vaia, R. A.; Giannelis, E. P. Macromolecules 1997, 30, 8000.
8. Kato, M.; Usuki, A.; Okada, A. J Appl Polym Sci 1997, 66, 1781.
9. Okada, A.; Fukoshima, Y.; Kawasumi, M.; Inagaki, S.; Usuki, A.; Sugiyama, S.; Kurauchi, T.; Kamigaito, O. U.S. Pat. 4,739,007 (1988).
10. Usuki, A.; Kawasumi, M.; Kojima, Y.; Fukoshima, Y.; Okada, A.; Kurauchi, T.; Kamigaito, O. J Mater Res 1993, 8, 1179.
11. Kojima, Y.; Usuki, A.; Kawasumi, M.; Okada, A.; Fukoshima, Y.; Kurauchi, T.; Kamigaito, O. J Mater Res 1993, 8, 1185.
12. Kojima, Y.; Usuki, A.; Kawasumi, M.; Okada, A.; Kurauchi, T.; Kamigaito, O. J Polym Sci Part A: Polym Chem 1993, 31, 983.
13. Giannelis, E. P. Adv Mater 1996, 8, 29.
14. Frisch, H. L.; Marck, J. E. Chem Mater 1996, 8, 1736.
15. Zilg, C.; Reichert, P.; Dietsche, F.; Engelhardt, T.; Mulhaupt, R. Kunstoffe 1998, 88, 1812.
16. Manias, E.; Touny, A.; Wu, L.; Strawhecker, K.; Lu, B.; Chung, T. C. Chem Mater 2001, 13, 3516.
17. Kato, M.; Usuki, A.; Okada, A. J Appl Polym Sci 1997, 66, 1781.
18. Hasegava, N.; Kawasumi, M.; Kato, M.; Usuki, A.; Okada, A. J Appl Polym Sci 1998, 67, 87.
19. Reichert, P.; Nitz, H.; Klinke, S.; Brandsch, R.; Thomann, R.; Mulhaupt, R. Macromol Mater Eng 2000, 275, 8.
20. Usuki, A.; Kato, M.; Okada, A.; Kurauchi, T. J Appl Polym Sci 1997, 63, 137.
21. Kawasami, M.; Hasegawa, N.; Kato, M.; Usuki, A.; Okada, A. Macromolecules 1997, 30, 6333.

22. Svoboda, P.; Zeng, C.; Wang, H. L.; Lee, J.; Tomasko, D. L. J Appl Polym Sci 2002, 85, 1562.
23. Hasegawa, N.; Usuki, A. J Appl Polym Sci 2004, 93, 464.
24. Wang, Y.; Chen, F.-B.; Wu, K.-C. J Appl Polym Sci 2005, 97, 1667.
25. Hasegawa, N.; Tsukigase, A.; Usuki, A. J Appl Polym Sci 2005, 98, 1554.
26. Lertwimolnun, W.; Vergnes, B. Polymer 2005, 46, 3462.
27. Ranade, A.; Nayak, K.; Fairbrother, D.; D'souza, N. A. Polymer 2005, 46, 7323.
28. Százdi, L.; Pukánszky, B.; Földes, E.; Pukánszky, B. Polymer 2005, 46, 8001.
29. Modesti, M.; Lorenzetti, A.; Bon, D.; Besco, S. Polymer 2005, 46, 10237.
30. Perrin-Sarazin, F.; Ton-That, M.-T.; Bureau, M. N.; Denault, J. Polymer 2005, 46, 11624.
31. Xu, W.; Liang, G.; Wang, W.; Tang, S.; He, P.; Pan, W.-P. J Appl Polym Sci 2003, 88, 3225.
32. Lee, J. W.; Kim, M. H.; Choi, W. M.; Park, O. O. J Appl Polym Sci 2006, 99, 1752.
33. Sinsawat, A.; Anderson, K. L.; Vaia, R. A.; Farmer, B. L. J Polym Sci Part B: Polym Phys 2003, 41, 3272.
34. Cho, K.; Li, F.; Choi, J. Polymer 1999, 40, 1719.
35. Ma, J.; Zhang, S.; Qi, Z.; Li, G.; Hu, Y. J Appl Polym Sci 2001, 83, 1978.
36. Dubnikova, I. L.; Berezina, S. M.; Oshmyan, V. G.; Kuleznev, V. N. J Polym Sci Part A: Polym Chem 2003, 45, 873.
37. Alexandre, M.; Dubois, P.; Sun, T.; Garces, J. M.; Jérôme, R. Polymer 2002, 43, 2123.
38. Ding, C.; Jia, D.; He, H.; Guo, B.; Hong, H. Polym Test 2005, 24, 94.
39. Dubnikova, I. L.; Berezina, S. M.; Yu, M. K.; Nikiforova, G. G. J Polym Sci Part A: Polym Chem 2005, 47, 1161.
40. Lomakin, S. M.; Zaikov, G. E. Modern Polymer Flame Retardancy; VSP International Science Publications: Utrecht, Boston, 2003; p 272.
41. Giannelis, E. Adv Mater 1996, 8, 29.
42. Gilman, J. W.; Kashiwagi, T.; Nyden, M. R.; Brown, J. E. T.; Jackson, C. L.; Lomakin, S. M.; Giannelis, E. P.; Manias, E. In Chemistry and Technology of Polymer Additives; Ak-Malaika, S., Golovoy, A., Wilkie, C. A., Eds.; Blackwell: Malden, 1999; Chapter 14, p 249.
43. Zanetti, M.; Kashiwagi, T.; Falqui, L.; Camino, G. Chem Mater 2002, 14, 881.
44. Kashiwagi, T.; Harris, R. H.; Zhang, X.; Briber, R. M.; Cipriano, B. H.; Raghavan, S. R.; Awad, W. H.; Shields, J. R. Polymer 2004, 45, 881.
45. Zanetti, M.; Lomakin, S.; Camino, G. Macromol Mater Eng 2000, 279, 1.
46. Hong, C. H.; Lee, Y. B.; Bae, J. W.; Jho, J. Y.; Nam, B. U.; Nam, G. J.; Lee, K. J. J Appl Polym Sci 2005, 97, 2375.
47. Qin, H.; Zhang, S.; Zhao, C.; Hu, G.; Yang, M. Polymer 2005, 46, 8386.
48. Lomakin, S. M.; Dubnikova, I. L.; Berezina, S. M.; Zaikov, G. E. Polym Int 2005, 54, 999.
49. Lomakin, S. M.; Dubnikova, I. L.; Berezina, S. M.; Zaikov, G. E.; Kozlowski, R.; Kim, G.-M.; Michler, G. H. In PPS-21 Annual Meeting of the Polymer Processing Society, Leipzig, Germany, June 19–23, 2005. SL12.8.
50. Lomakin, S. M.; Dubnikova, I. L.; Berezina, S. M.; Zaikov, G. E. J Polym Sci Part A: Polym Chem 2006, 48, 72.